

Crystalline lens gradient refractive index distribution in the guinea pig

Alberto de Castro¹ , Eduardo Martínez-Enríquez¹ , Pablo Pérez-Merino¹ , Miriam Velasco-Ocaña¹, Luis Revuelta² , Sally McFadden³  and Susana Marcos¹ 

¹Instituto de Óptica “Daza de Valdés”, Consejo Superior de Investigaciones Científicas (IO-CSIC), Madrid, Spain, ²Facultad de Veterinaria, Universidad Complutense de Madrid (UCM), Madrid, Spain, and ³Vision Sciences, School of Psychology and Hunter Medical Research Institute, University of Newcastle, Newcastle, NSW, Australia

Citation information: de Castro A, Martínez-Enríquez E, Pérez-Merino P, Velasco-Ocaña M, Revuelta L, McFadden S, & Marcos S. Crystalline lens gradient refractive index distribution in the guinea pig. *Ophthalmic Physiol Opt* 2020; 40: 308–315. <https://doi.org/10.1111/opo.12667>

Keywords: guinea pig, crystalline lens, gradient refractive index, myopia

Correspondence: Alberto de Castro
E-mail address: a.decastro@csic.es

Received: 20 September 2019; Accepted: 4 December 2019

Author contributions: AdC and EM: involved in data analysis and interpretation; drafting and critically revising the manuscript. PP, MV, LR and SMcF: involved in data acquisition; critically revising the manuscript. SMcF and SM: involved in study conception and design; data interpretation; drafting and critically revising the manuscript.

Abstract

Purpose: The crystalline lens undergoes morphological and functional changes with age and may also play a role in eye emmetropisation. Both the geometry and the gradient index of refraction (GRIN) distribution contribute to the lens optical properties. We studied the lens GRIN in the guinea pig, a common animal model to study myopia.

Methods: Lenses were extracted from guinea pigs (*Cavia porcellus*) at 18 days of age ($n = 4$, three monolaterally treated with negative lenses and one untreated) and 39 days of age ($n = 4$, all untreated). Treated eyes were myopic (-2.07 D on average) and untreated eyes hyperopic ($+3.3$ D), as revealed using streak retinoscopy in the live cyclopeded animals. A custom 3D spectral domain optical coherence tomography (OCT) system ($\lambda = 840$ nm, $\Delta\lambda = 50$ nm) was used to image the enucleated crystalline lens at two orientations. Custom algorithms were used to estimate the lens shape and GRIN was modelled with four variables that were reconstructed using the OCT data and a minimisation algorithm. Ray tracing was used to calculate the optical power and spherical aberration assuming a homogeneous refractive index or the estimated GRIN.

Results: Guinea pig lenses exhibited nearly parabolic GRIN profiles. When comparing the two age groups (18- and 39 day-old) there was a significant increase in the central thickness (from 3.61 to 3.74 mm), and in the refractive index of the surface (from 1.362 to 1.366) and the nucleus (from 1.443 to 1.454). The presence of GRIN shifted the spherical aberration (-4.1 μm on average) of the lens towards negative values.

Conclusions: The guinea pig lens exhibits a GRIN profile with surface and nucleus refractive indices that increase slightly during the first weeks of life. GRIN plays a major role in the lens optical properties and should be incorporated into computational guinea pig eye models to study emmetropisation, myopia development and ageing.

Introduction

The crystalline lens of the eye is a biconvex optical element with aspheric surfaces and a gradient index of refraction (GRIN). In combination with the cornea it focuses the light from the outside world onto the retina in the emmetropic eye and changes its power to focus near and far objects. In addition, in many species, including human, the lens

compensates the spherical aberration of the cornea improving the quality of the retinal image.

The coordination between the changing optics and the eyes elongation to achieve best focus on the retina during eye growth in childhood, is known as emmetropisation. This coordination is disrupted in myopia. The main biometric difference between myopic and emmetropic eyes is its axial length, however, differences in the crystalline lens have also

been reported. It is known that the lens power in myopic children is lower than in emmetropes¹ and that within one year of the onset of myopia the crystalline lens stops thinning, flattening and losing power.² In a previous study we found that in humans, the refractive error and the lens equatorial diameter were correlated in young adults³ perhaps due to ciliary muscle and/or associated equatorial changes contributing to lens flattening.

The guinea pig is an accessible mammalian model popular for studying myopia development, as it has been shown to respond efficiently to diffusers⁴ or lens treatments⁵ developing refractive errors. The main difference between treated and untreated eyes is the axial length but changes in the lens thickness have also been reported.⁵

In our group we have showed that anterior segment optical coherence tomography (OCT) imaging can be used to assess crystalline lens geometrical parameters,^{6,7} and that it is possible to reconstruct the crystalline lens GRIN *in vitro* using images of the *in vitro* crystalline lens in two orientations, first with the anterior surface facing the OCT beam (anterior-up image) and then with the posterior surface facing the OCT beam (posterior-up image).⁸ Essentially, a global optimisation technique is used to optimise the value of the variables of a GRIN model so that the simulated optical path matches the one measured from the OCT images. We have demonstrated the technique in an isolated porcine crystalline lens,⁸ in cynomolgus monkey lenses,^{9,10} and in human lenses of different ages.^{11,12}

Computer models based on the geometry of the guinea pig eye are useful to understand the relative contribution of the ocular components and axial distances to refractive error and optical quality, particularly during eye growth. In the past, guinea pig eye models were constructed using geometrical parameters obtained from frozen sections.¹³ More recently, we generated anatomical computer models of the guinea pig eye, using individual measurements of the anterior and posterior corneal and lens surface topographies, anterior chamber depth and axial length, all obtained three-dimensionally from the same OCT volume.¹⁴ The indices of refraction of the cornea, aqueous and vitreous humors, and a hypothetical homogeneous crystalline lens (1.376, 1.3346 and 1.401 respectively) were obtained from the literature¹³ and a good correspondence between the spherical error predicted from the calculated optical power and the axial length obtained using geometrical measurements from OCT was found. However, optical aberrations were also characterised *in vivo*, and the spherical aberration measured and predicted in the same eyes was dramatically different (positive from the virtual ray tracing estimates, and negative from the experimental aberrometry measurements).¹⁴ In that work, we hypothesised that the source of the discrepancy was the presence of a GRIN in the crystalline lens, not accounted for in the simulations.

In this study, we reconstructed the GRIN of the isolated guinea pig crystalline lens (excised from untreated and myopia-treated eyes at two different ages) and compared the spherical aberration of the lens with the reconstructed GRIN and with a homogeneous refractive index.

Methods

Wild-type tri-colored animals were obtained from a farm and raised in a 12/12 h light/dark cycle in the animal facility of the Facultad de Veterinaria, Universidad Complutense, Madrid, Spain (FV-UCM). Protocols were approved by the FV-UCM Ethical Committee and adhered to the Association for Research in Vision and Ophthalmology (ARVO) Statement for the Use of Animals in Ophthalmic and Vision Research.

Eight pigmented guinea pig (*Cavia porcellus*) eyes were studied at 18 (three animals, four eyes) and 39 (four animals, four eyes) days of age. In the 18-day group the right eye of three animals had been treated with a -6 D lens for two weeks (from 4 to 18 days of age)⁵ and the three treated eyes and one untreated left eye were studied. In the older group the four lenses were extracted from untreated eyes in four animals. The animals were euthanised by a cardiac injection with an overdose of pento-barbitone prior to eye enucleation. The crystalline lens was isolated and imaged in the OCT immediately following enucleation.

All the 18-day-old animals were refracted *in vivo* before euthanasia using white light streak retinoscopy⁴ without cycloplegia. Treated eyes in the 18-day-old group were myopic (-3.5 , -2.8 , -0.2 D and the non-treated eye was hyperopic ($+3.3$ D). The refractive error of the untreated eyes in the 39-day-old animals was not measured. However, the emmetropisation process of the guinea pig was characterized in a study by Howlet and McFadden, which showed that the mean refractive error in untreated animals at day 39 is, on average, $+0.7$ D.¹⁴

Isolated crystalline lenses were placed in a cuvette filled with balanced salt solution and immediately imaged in a custom 3D spectral OCT system. A mirror was used to tilt the beam 90 degrees and allow scanning the lens in a horizontal position with the beam illuminating from above. The OCT instrument, and the algorithms for automatic image processing and fan and optical distortion correction have been described in a previous publication¹⁵. Briefly, the set-up is based on a Fiber-Optic Michelson Interferometer with a super-luminescent diode light source ($\lambda_0 = 840$ nm, $\Delta\lambda = 50$ nm), and a spectrometer consisting of a volume diffraction grating and a complementary metal-oxide-semiconductor (CMOS) camera. The effective acquisition speed was 25000 A-scans/s and the axial range was 7 mm. The axial pixel size and nominal resolution in tissue were 3.4 and 6.9 μm , respectively.

3D images of the lens were acquired using 70 B-scans of 1667 A-scans each in a region of 8×8 mm resulting in a pixel size of 114×4.8 μm in the horizontal and vertical directions respectively. First, an image of the lens with the anterior surface facing the OCT beam (anterior-up image) was captured. The crystalline lens was then flipped over and a second image of the lens was captured with the posterior surface facing the OCT beam (posterior-up). The geometry of the lens was measured using the first surface in each image (anterior in anterior-up and posterior in the posterior-up). The image of the second surface (posterior in anterior-up and anterior in posterior-up) is distorted but contains the information of the optical path of the rays that was used to reconstruct the lens GRIN. The surface of the cuvette, visible in the images, was also used as input for the GRIN reconstruction algorithm and allowed to measure the thickness of the lens¹⁶ and to register the volumes correcting for possible rotations when flipping the lens.⁸

The surfaces of the lens and the cuvette were segmented and the fan-distortion due to the scanning architecture was corrected using custom signal processing software.¹⁵ The anterior and posterior surfaces of the crystalline lens were fitted by conics in the central 4-mm pupil obtaining two parameters: the radius of curvature at the vertex, r , and the shape factor, p , which is a function of the eccentricity of the conic surface ($p < 0$ for hyperboloids, $p = 0$ for paraboloids, $p = 1$ for spherical surfaces).

The GRIN distribution was modelled using a 4-variable equation that describes the continuous change of the refractive index from nucleus to surface (see Figure 1) with the equation:

$$n(\rho, \theta) = n_N - \Delta n \cdot \left(\frac{\rho}{\rho_S(\theta)} \right)^{p(\theta)},$$

where ρ and θ are polar coordinates referenced to the lens center, which we positioned on the optical axis at a distance from the anterior surface of 0.41 times the thickness of the lens,¹⁷ $\rho_S(\theta)$ is the distance from the center to the surface, n_N is the nucleus refractive index, $\Delta n = n_N - n_S$, n_S is the surface refractive index, and $p(\theta)$ represents the exponent of the power law which can be different in the axial ($\theta = 0$, $p1$) and in the meridional ($\theta = 90$ degrees, $p2$) directions.

The optimisation algorithm used to find the variables of the GRIN model that best matched the experimental data has been previously described in detail.⁸ It is based on a genetic search and uses as input data the geometry of the anterior and posterior crystalline lens surface, the lens thickness, the group refractive index of the preservation media, 1.345 at the OCT wavelength, and the distorted surfaces of the posterior surface of the lens and the cuvette visible in the OCT images. Custom algorithms were developed

in MATLAB (www.mathworks.com) to combine standard routines for ray tracing through conical surfaces with either homogeneous¹⁸ or GRIN media^{19,20} and to calculate the optical path accumulated by the rays when passing through the lens. The algorithms were validated against OpticStudio optical design commercial software (www.zemax.com).²¹ Due to the broad band light source of the imaging system, 50 nm, the output of the optimisation algorithm corresponds to the group refractive index at the OCT central wavelength, 840 nm. While the phase refractive index of a medium is the ratio between the speed of light in vacuum and the phase velocity in the medium, the group refractive index is defined with the velocity of the group or waves, that is, the envelope of the wave's amplitude. There is a mathematical relation between both refractive indices¹⁷ and in this study, the reconstructed values were first transformed from group to phase refractive index at 840 nm and then to phase refractive index at 630 nm.¹⁶

The equivalent refractive index, i.e. the homogeneous refractive index of a lens with the same external geometry and dioptrical power as the crystalline lens, was calculated using the ray tracing program and the optics of the crystalline lens with the GRIN and the homogeneous refractive index compared. The paraxial and non-paraxial crystalline lens optical power and the wave aberration of each lens was calculated using the algorithms to trace rays through the measured external geometry and either the reconstructed GRIN or the homogeneous equivalent refractive index. The wave aberration was then fitted by Zernike polynomial expansions up to the 6th order. All calculations were performed for 4-mm pupil diameters, which is close to the natural pupil size of the guinea pig eye¹³.

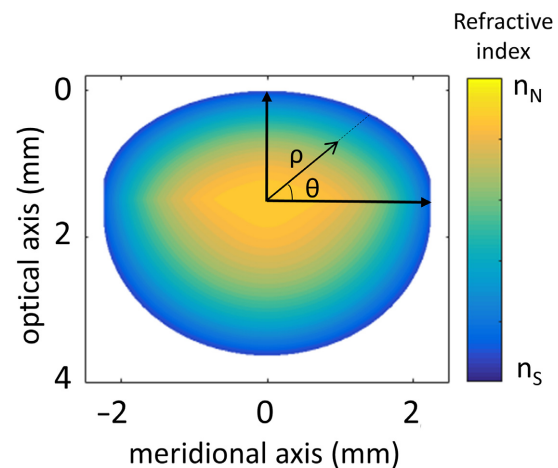


Figure 1. Gradient refractive index (GRIN) is described in each meridian by four variables: nucleus and surface refractive index and axial and meridional exponent power laws. The center of the lens is positioned in the optical axis at a distance from the anterior surface of 0.41 times the lens thickness and the GRIN was calculated using equation 1.

Results

Figure 2 shows the lens anterior surface (in cyan), lens posterior surface (in red) and the surface of the cuvette (in black) with solid lines indicating the real geometry and dashed lines indicating the surface as observed in the raw OCT images. The corresponding GRIN profiles for the eight crystalline lenses is superimposed. All values correspond to phase refractive index at 630 nm. The reconstructed surface refractive indices ranged between 1.371 and 1.378, the nucleus refractive indices between 1.451 and 1.466, the meridional power exponent between 2.367 and 5.913 and the axial power exponent between 1.912 and 2.100. The values of the equivalent refractive index ranged from 1.431 and 1.465. Figure 3 illustrates the untreated 18-day-old (Figure 3a) and one of the 39-day-old guinea pig lenses (Figure 3b) in the axial direction and in 17 lens meridians (from 0 to 180 in steps of 5 degrees). When comparing the two ages, it can be observed that the nucleus refractive index of the 39-day old guinea pig was about 0.01 larger than that of the 18-day old although the shape of the

refractive index profile was similar. The similarity of the profiles across meridians indicates that there is a high degree of symmetry around the lens optical axis.

A comparison between age groups was done for all the GRIN parameters (Figure 4). When compared with the 18-day-old, 39-day-old lenses exhibit a statistically higher surface refractive index (1.366 ± 0.002 vs 1.362 ± 0.001 ; two-tailed t -test $p = 0.010$) and nucleus refractive index (1.454 ± 0.004 vs 1.443 ± 0.002 ; $p = 0.003$) (Figure 4a). In the 18-day-old group there were untreated and treated eyes but the surface and nucleus refractive index in the older animals (all non-myopic) were all higher than the corresponding refractive index in the untreated 18-day-old guinea pig eye (surface 1.363 nucleus 1.443). The exponential decays in the axial and meridional directions were not statistically different between age groups (Figure 4b). As a result of the differences in the GRIN, the equivalent refractive index was statistically higher in the 39-day-old group of lenses (1.461 ± 0.004 vs 1.440 ± 0.006 ; $p = 0.001$).

We studied the differences in external geometry between groups (Figure 5) and found that older lenses were

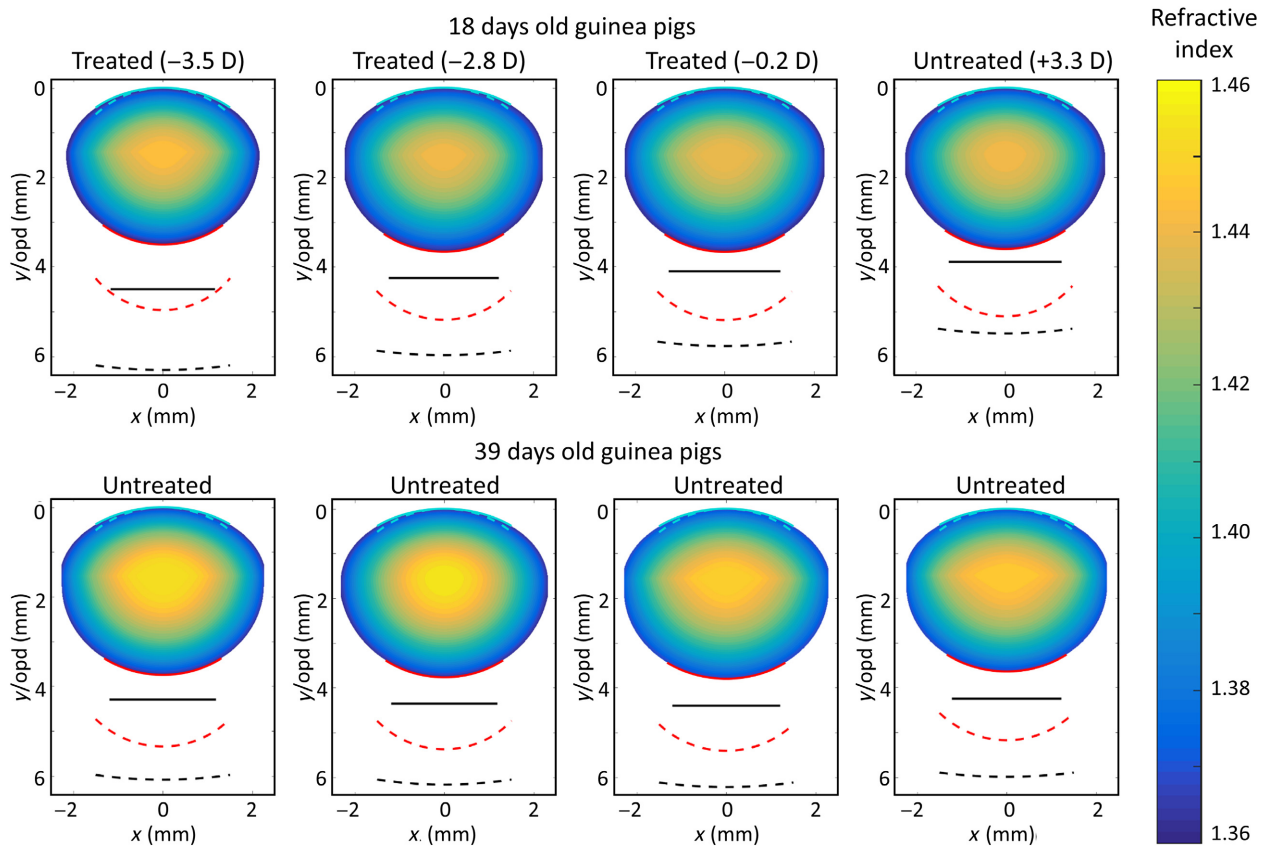


Figure 2. Reconstructed color-coded GRIN in the eight lenses of the study, anterior lens surface (in cyan), posterior lens surface (in red) and surface of the cuvette holding the lens and the preservation media (in black). The real geometry (solid lines) and the surfaces as observed in the raw OCT images (dashed lines) are presented. The figure shows a meridional section of the lens with the horizontal axis representing the distance to the lens center and the vertical axis representing both the geometrical distance, y , and the optical path of the rays, opd .

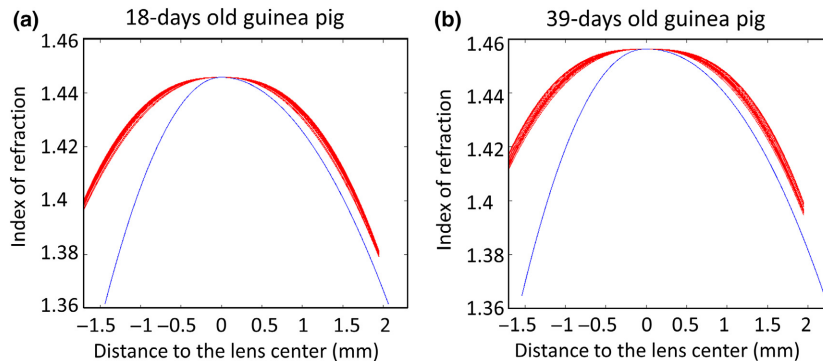


Figure 3. Crystalline lens gradient refractive index profile in the axial (blue) and meridional (red) directions of two untreated animals at (a) 18- and (b) 39-days old. In the blue curve, negative values in the horizontal axis correspond to the anterior part of the lens and positive to the posterior. The crystalline lens nucleus refractive index is higher in the 38-day old guinea pig.

significantly thicker (by 130 μm on average, $p = 0.047$). Though the difference was not significant, we noticed a that the posterior surface tended to flatten (radius of curvature difference of 178 μm , $p = 0.060$).

The crystalline lens shape parameters did not change significantly with the eye refractive error. However, we observed a tendency of the surfaces to be steeper in myopes, both when studying only the 18-day-old group (0.533 mm D^{-1} for the anterior surface and 0.848 mm D^{-1} for the posterior surface) and when including both the 18- and the 39-day old group and assuming a refractive error of +0.7 D¹³ for the latter (0.562 mm D^{-1} for the anterior surface and 0.713 mm D^{-1} for the posterior surface). The experimental data (see Figure 6) also show a tendency of the lens to thicken with myopia (0.584 mm D^{-1} for the 18-day group only; 0.579 mm D^{-1} for all eyes).

Calculations of the focal length, optical power and spherical aberration were done using the measured surface geometry and the reconstructed GRIN parameters. Paraxial back focal length ranged from 7.79 to 9.87 mm, and non-paraxial back focal length for a 4 mm pupil ranged from 8.96 to 10.64 mm. This represents an optical power from 85.6 to 104.7 D for paraxial and 80.2 to 92.3 D for a 4 mm pupil.

Figure 7 shows the spherical aberration of the crystalline lens with the reconstructed GRIN (values range from -14.9 to -1.9 and from -11.6 to 16.7 μm , for the 18- and the 39-day-old lenses respectively) and with the calculated homogeneous equivalent refractive index (values range from 31.3 to 33.5 and from 29.9 to 32.4 μm , for the 18- and 39-day-old lenses respectively). The presence of GRIN shifts the value of the spherical aberration towards more negative values. Also, while the spherical aberration does not show a significant age dependency, the lens spherical aberration is, on average, lower in the 18-day-old than in the 39-day-old group. The crystalline lens spherical aberration results were not correlated with the eye refractive error.

Discussion

We used an OCT-based method to measure the shape and the gradient index structure of the in vitro guinea pig crystalline lens. We found that the crystalline lens of the guinea pig eye exhibits a gradient index structure with a relatively large variation of the index of refraction from the nucleus to the periphery (on average 1.365 in the surface, 1.449 in

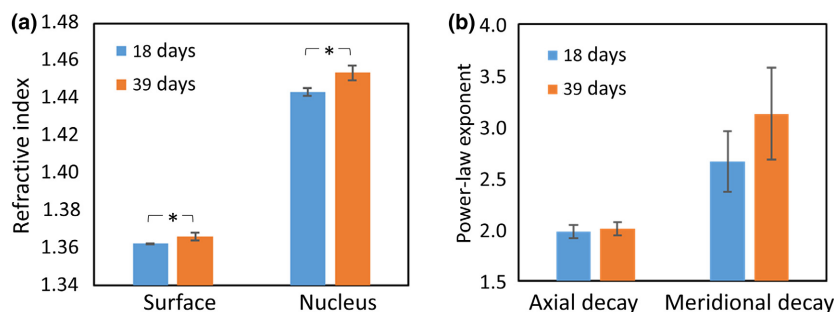


Figure 4. Gradient index of refraction (GRIN) parameters for 18-day-old (blue bars) and 39-day-old (orange bars) guinea pigs. (a) Surface and nucleus refractive index; (b) axial and meridional decay. The asterisk indicates that the difference between groups is statistically significant ($p,0.05$).

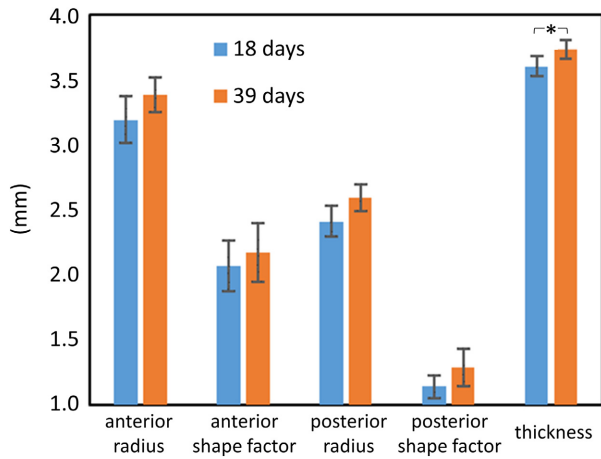


Figure 5. Comparison of the geometry between lenses extracted from the 18-day old (blue bars) and the 39-day old (orange bars) guinea pigs. The asterisk indicates that the difference between groups is statistically significant. Both surfaces are on average flatter in older lenses and there is a statistically significant increase in the crystalline lens central thickness.

the nucleus, 0.084 difference), and a nearly parabolic profile (average exponent decay coefficient of 2.00 and 2.98 in the axial and meridional directions respectively). We studied the differences between two age groups, 18- and 39-days old, before the sexual maturity which occurs on average at 75 days for these animals.¹³ The 39-day-old lenses exhibited higher surface and nucleus refractive indices and a higher equivalent refractive index. GRIN was found to reduce the spherical aberration of the lens (on average from 31.6 to $-4.1 \mu\text{m}$), making it negative in the 18-day-old group.

To our knowledge, there is only one previous report of measurements of the guinea pig crystalline lens GRIN.²² The measurement was performed probing with a waveguide different locations of the lens and estimating the local refractive index from the Fresnel reflectance coefficient at 670 nm in a single animal. The study reported refractive

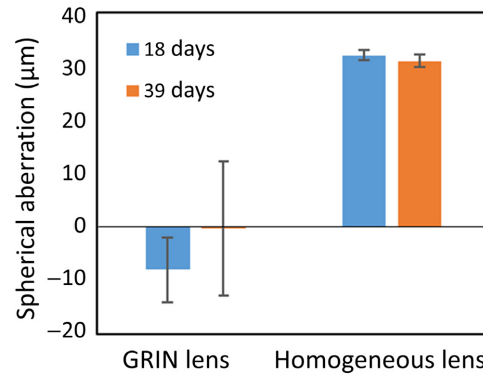


Figure 7. Spherical aberration with the reconstructed gradient index of refraction (GRIN) and with the equivalent refractive index. The gradient index of refraction shifts the spherical aberration of the lens toward negative values.

indices for surface and nucleus (1.389 and 1.429) that are respectively higher and smaller than the values found here (on average 1.363 and 1.447 for 670 nm light). In the rat, an animal of similar size, the GRIN was studied with a ray tracing method²³ and the values, reported for 589 nm wavelength, 1.336 and 1.508 for surface and nucleus respectively are comparable to our results (on average 1.366 and 1.450 for surface and nucleus when converted to 589 nm wavelength). Also, the shape of the refractive index profile that we found agrees well with the parabolic profile reported in those two studies.^{22,23}

The GRIN distribution in the guinea pig lens is close to that found in other mammals, although the values of refractive index are somewhat higher. In porcine lenses, using a ray tracing tomographic method values for surface/nucleus of 1.366/1.444 were reported. With our method we found 1.362/1.443 in porcine lenses,⁸ 1.370/1.429 in cynomolgus monkey lenses⁹; and 1.360/1.425 in humans.¹²

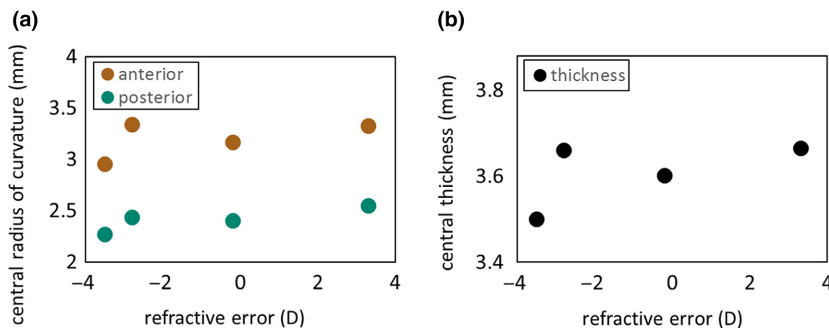


Figure 6. Crystalline lens shape parameters were not correlated with refractive error ($p > 0.05$). (a) Anterior and posterior apical radius of curvature; (b) central lens thickness of the four 18-day old guinea pigs.

Our prior studies also found parabolic profiles (i.e. exponential decays close to 2) in porcine (2.6), and in the young human lens (close to 2 in the axial direction).

The output of the optimisation algorithm is the group refractive index at the OCT wavelength and was transformed into phase refractive index at a visible wavelength¹⁶ using dispersion curves that were derived indirectly for humans.²⁴ To estimate the approximation of using these curves in the guinea pig we calculated the result of the transformation when using the water dispersion curves²⁵ and found a difference of only 0.0002 in the resulting phase refractive index.

The effect of GRIN on lens power and on the spherical aberration in the guinea pig lens was similar to that found in fish, porcine, cynomolgus monkeys and young humans. The paraxial and non-paraxial optical power for a 4-mm pupil diameter of the surfaces was on average 13.7 and 14.7 D respectively, indicating that GRIN contributes more than 80% (on average 85.5% and 80.9% to paraxial and non-paraxial power respectively) to the lens optical power. Also GRIN shifts the spherical aberration to lower (and even negative) values with respect to the spherical aberration of a lens with the same geometry and a constant index of refraction. The spherical aberration values estimated for the guinea pig lens are around an order of magnitude higher than those found in isolated human, porcine or monkey lenses, to a large extent because of much steeper surfaces. Unlike in human and cynomolgus monkey lenses, where the posterior lens asphericity is negative, the guinea pig lens asphericities were positive. Interestingly, the impact of GRIN in the lens spherical aberration is reduced in the 39-day group when compared to the emmetropic eye in the 18-day group. The lens optical power remained constant with age despite the posterior radius of curvature increase, suggesting a compensatory role of GRIN which resembles, in part, the lens paradox in humans.^{26–28}

GRIN measurements were obtained on excised lenses, with released tension from the zonulae. Whether the guinea pig lens can accommodate or not is a matter of debate, and therefore we do not know if geometrical differences are expected between the *in vivo* and *in vitro* (nominally maximally accommodated) conditions. In any case, we do not expect this fact to affect the estimated GRIN parameters, as a previous study did not show significant differences in nucleus or surface refractive indices or shape factor with accommodation in cynomolgus monkey lenses mounted in a stretcher.¹⁰

Knowledge of the crystalline lens GRIN as reported here, will improve computer eye models of the guinea pig eye, such as those we described previously,¹⁴ where a comparison of experimental and predicted aberrations showed a discrepancy in the sign of the spherical aberration. Incorporation of the GRIN in eye models will allow realistic

predictions of spherical aberration and increased accuracy in the estimation of the guinea pig posterior crystalline lens shape *in vivo*.^{29,30}

While our sample was not sufficiently large to investigate crystalline lens changes with refractive error, a full characterisation of the GRIN will further allow understanding the role of crystalline lens morphology and structure in lens emmetropisation. Also, it will help to understand the potential of the accommodation mechanism in the guinea pig eye, still largely unexplored.

In summary, we have presented for the first time a study on the external geometry and gradient refractive index of the guinea pig crystalline lens and we have studied its influence in the optics of the lens. In these animals, GRIN seems to play a role in the optical quality of the eye, maintaining the optical power of the lens with age and may be responsible for some of the changes in spherical aberration with age.

Acknowledgements

This work was supported by European Research Council (ERC) Grant Agreement ERC-2011-AdC- 294099; ERC under the European Union's Horizon 2020 research and innovation programme (H2020-MSCA COFUND-2015 FP-713694, MULTIPLY) and under grant agreement No 779960, IMCUSTOMEYE and No 675137 (MyFUun MSCA ITN); Spanish Government Grant FIS2017-84753-R; Hunter Medical Research Institute G1400967 and the University of Newcastle (FVG 1031537 and SSP).

Conflicts of interest

The authors report no conflicts of interest and have no proprietary interest in any of the materials mentioned in this article.

References

1. Garner LF, Yap M & Scott R. Crystalline lens power in myopia. *Optom Vis Sci* 1992; 69: 863–865.
2. Mutti DO, Mitchell GL, Sinnott LT *et al.* Corneal and crystalline lens dimensions before and after myopia onset. *Optom Vis Sci* 2012; 89: 251–262.
3. Muralidharan G, Martinez-Enriquez E, Birkenfeld J, Velasco-Ocana M, Pérez-Merino P & Marcos S. Morphological changes of human crystalline lens in myopia. *Biomed Opt Express* 2019; 10: 6084–6095.
4. Howlett MHC & McFadden SA. Form-deprivation myopia in the guinea pig (*Cavia porcellus*). *Vision Res* 2006; 46: 267–283.
5. Howlett MHC & McFadden SA. Spectacle lens compensation in the pigmented guinea pig. *Vision Res* 2009; 49: 219–227.

6. Ortiz S, Pérez-Merino P, Gamba E, de Castro A & Marcos S. *In vivo* human crystalline lens topography. *Biomed Opt Express* 2012; 3: 2471–2488.
7. Martínez-Enriquez E, Sun M, Velasco-Ocana M, Birkenfeld J, Pérez-Merino P & Marcos S. Optical coherence tomography based estimates of crystalline lens volume, equatorial diameter, and plane position. *Invest Ophthalmol Vis Sci* 2016; 57: 600–610.
8. de Castro A, Ortiz S, Gamba E, Siedlecki D & Marcos S. Three-dimensional reconstruction of the crystalline lens gradient index distribution from OCT imaging. *Opt Express* 2010; 18: 21905–21917.
9. de Castro A, Birkenfeld J, Maceo B *et al.* Influence of shape and gradient refractive index in the accommodative changes of spherical aberration in nonhuman primate crystalline lenses. *Invest Ophthalmol Vis Sci* 2013; 54: 6197–6207.
10. de Castro A, Birkenfeld J, Heilman BM *et al.* Off-axis optical coherence tomography imaging of the crystalline lens to reconstruct the gradient refractive index using optical methods. *Biomed Opt Express* 2019; 10: 3622–3634.
11. de Castro A, Siedlecki D, Borja D *et al.* Age-dependent variation of the Gradient Index profile in human crystalline lenses. *J Mod Opt* 2011; 58: 1781–1787.
12. Birkenfeld J, de Castro A & Marcos S. Contribution of shape and gradient refractive index to the spherical aberration of isolated human lenses. *Invest Ophthalmol Vis Sci* 2014; 55: 2599–2607.
13. Howlett MH & McFadden SA. Emmetropization and schematic eye models in developing pigmented guinea pigs. *Vision Res* 2007; 47: 1178–1190.
14. Pérez-Merino P, Velasco-Ocana M, Martínez-Enriquez E *et al.* Three-dimensional OCT based guinea pig eye model: relating morphology and optics. *Biomed Opt Express* 2017; 8: 2173–2184.
15. Martínez-Enriquez E, Pérez-Merino P, Velasco-Ocana M & Marcos S. OCT-based full crystalline lens shape change during accommodation in vivo. *Biomed Opt Express* 2017; 8: 918–933.
16. Uhlhorn SR, Borja D & Parel JM. Refractive index measurement of the isolated crystalline lens using optical coherence tomography. *Vision Res* 2008; 48: 2732–2738.
17. Rosen AM, Denham DB, Fernandez V *et al.* In vitro dimensions and curvatures of human lenses. *Vision Res* 2006; 46: 1002–1009.
18. Stavroudis OO. *The Optics of Rays, Wavefronts and Caustics*, Academic Press: New York, 1972.
19. Sharma A, Kumar DV & Ghatak AK. Tracing rays through graded-index media - a new method. *Appl Optics* 1982; 21: 984–987.
20. Stone BD & Forbes GW. Optimal interpolants for Runge-Kutta ray tracing in inhomogeneous-media. *J Opt Soc Am A* 1990; 7: 248–254.
21. de Castro A, Barbero S & Marcos S. Accuracy of the reconstruction of the crystalline lens gradient index with optimization methods from ray tracing and Optical Coherence Tomography data. *Opt Express* 2011; 19: 19265–19279.
22. Pierscionek B. Species variations in the refractive index of the eye lens and patterns of change with ageing. In: *Focus on Eye Research*, OR Ioseliani, (ed.). Nova Science Publishers, Inc. New York, 2005; pp. 91–115.
23. Campbell MC. Measurement of refractive index in an intact crystalline lens. *Vision Res* 1984; 24: 409–415.
24. Atchison DA & Smith G. Chromatic dispersions of the ocular media of human eyes. *J Opt Soc Am A Opt Image Sci Vis* 2005; 22: 29–37.
25. Daimon M, Masumura A. Measurement of the refractive index of distilled water from the near-infrared region to the ultraviolet region. *Appl Optics* 2007; 46: 3811–3820.
26. Dubbelman M & Van der Heijde GL. The shape of the aging human lens: curvature, equivalent refractive index and the lens paradox. *Vision Res* 2001; 41: 1867–1877.
27. Moffat BA, Atchison DA & Pope JM. Explanation of the lens paradox. *Optom Vis Sci* 2002; 79: 148–150.
28. Sheil CJ & Goncharov AV. Crystalline lens paradoxes revisited: significance of age-related restructuring of the GRIN. *Biomed Opt Express* 2017; 8: 4172–4180.
29. Siedlecki D, de Castro A, Gamba E *et al.* Distortion correction of OCT images of the crystalline lens: gradient index approach. *Optom Vis Sci* 2012; 89: E709–E718.
30. Borja D, Siedlecki D, de Castro A *et al.* Distortions of the posterior surface in optical coherence tomography images of the isolated crystalline lens: effect of the lens index gradient. *Biomed Opt Express* 2010; 1: 1331–1340.